



HAL
open science

Seasonal and event-based concentration-discharge relationships to identify catchment controls on nutrient export regimes

Camille Minaudo, Rémi Dupas, Chantal Gascuel, Vincent Roubeix, Pierre-Alain Danis, Florentina Moatar

► To cite this version:

Camille Minaudo, Rémi Dupas, Chantal Gascuel, Vincent Roubeix, Pierre-Alain Danis, et al.. Seasonal and event-based concentration-discharge relationships to identify catchment controls on nutrient export regimes. *Advances in Water Resources*, 2019, 131, pp.103379. <10.1016/j.advwatres.2019.103379>. <hal-02377278>

HAL Id: hal-02377278

<https://hal.science/hal-02377278v1>

Submitted on 25 Oct 2021

HAL is a multi-disciplinary open access archive for the deposit and dissemination of scientific research documents, whether they are published or not. The documents may come from teaching and research institutions in France or abroad, or from public or private research centers.

L'archive ouverte pluridisciplinaire **HAL**, est destinée au dépôt et à la diffusion de documents scientifiques de niveau recherche, publiés ou non, émanant des établissements d'enseignement et de recherche français ou étrangers, des laboratoires publics ou privés.



Distributed under a Creative Commons CC BY-NC 4.0 - Attribution - Non-commercial use - International License

1 Seasonal and event-based concentration-discharge relationships to identify 2 catchment controls on nutrient export regimes

3 Camille Minaudo^{1,2}, Rémi Dupas³, Chantal Gascuel-Oudou³, Vincent Roubeix⁴, Pierre-Alain
4 Danis⁵, Florentina Moatar^{2,6}

5 1. Physics of Aquatic Systems Laboratory, EPFL, Lausanne, Switzerland

6 2. E.A. 6293 GeHCO, University François Rabelais of Tours, Tours, France

7 3. INRA UMR 1069 SAS, Rennes, France

8 4. IRSTEA, UR RECOVER, Pôle AFB-Irstea Hydroécologie plans d'eau, Aix-en-Provence, France

9 5. Agence Française pour la Biodiversité, Pôle AFB-Irstea Hydroécologie plans d'eau, Aix-en-Provence, France

10 6. RiverLy-IRSTEA, Lyon, France

11 Corresponding author: camille.minaudo@epfl.ch

12 Abstract

13 The analysis of concentration-discharge (C-Q) relationships provides useful information on
14 the processes controlling the mobilization and delivery of chemical elements into streams as
15 well as biogeochemical transformations in river networks. Previous metrics developed to
16 characterize export regimes seldom considered the possibility for the C response to Q
17 dynamics to differ between short-term Q variations during storm events and seasonal Q
18 variations during baseflow periods. Here, we present the “C-Q_{quick-slow}” model, which
19 considers the possibility for C-Q relationships to vary across temporal scales. This model was
20 applied in 219 French catchments with various sizes (11 – 2500 km²), land use and
21 hydrological contexts. We evidenced contrasting export regimes for nitrate (NO₃⁻), total
22 phosphorus (TP) and soluble reactive phosphorus (SRP), and surprisingly consistent C-Q
23 patterns at the seasonal scale for each parameter. For instance, NO₃⁻-Q relationships were
24 positive at the seasonal scale in 75% cases and relationships during storms showed either a
25 dilution pattern (24% cases), a non-significant pattern (50%), or a mobilization pattern (12%).
26 TP and SRP relationships with Q at the seasonal scale were almost systematically negative
27 (95%), and patterns during storm events were in most cases mobilization for TP (77%) or
28 non-significant for SRP (69%). We linked the different C-Q relationships with catchment
29 descriptors and found that indicators of diffuse source loading determined NO₃⁻ seasonal
30 amplitudes, and hydrological drivers could explain the behavior during storms. By contrast,
31 point sources determined P seasonal amplitudes, and diffuse sources controlled P dynamics
32 during storms. The C-Q_{quick-slow} model has the potential to improve nutrient load estimations
33 because of the good predictability of appropriate C-Q archetypes and the possibility to
34 interpolate low frequency concentration data to a daily frequency.

35 **Keywords:** concentration-discharge relationships, nutrient export regime, spatial variability;
36 eutrophication, nitrogen, phosphorus, catchment, river network

37

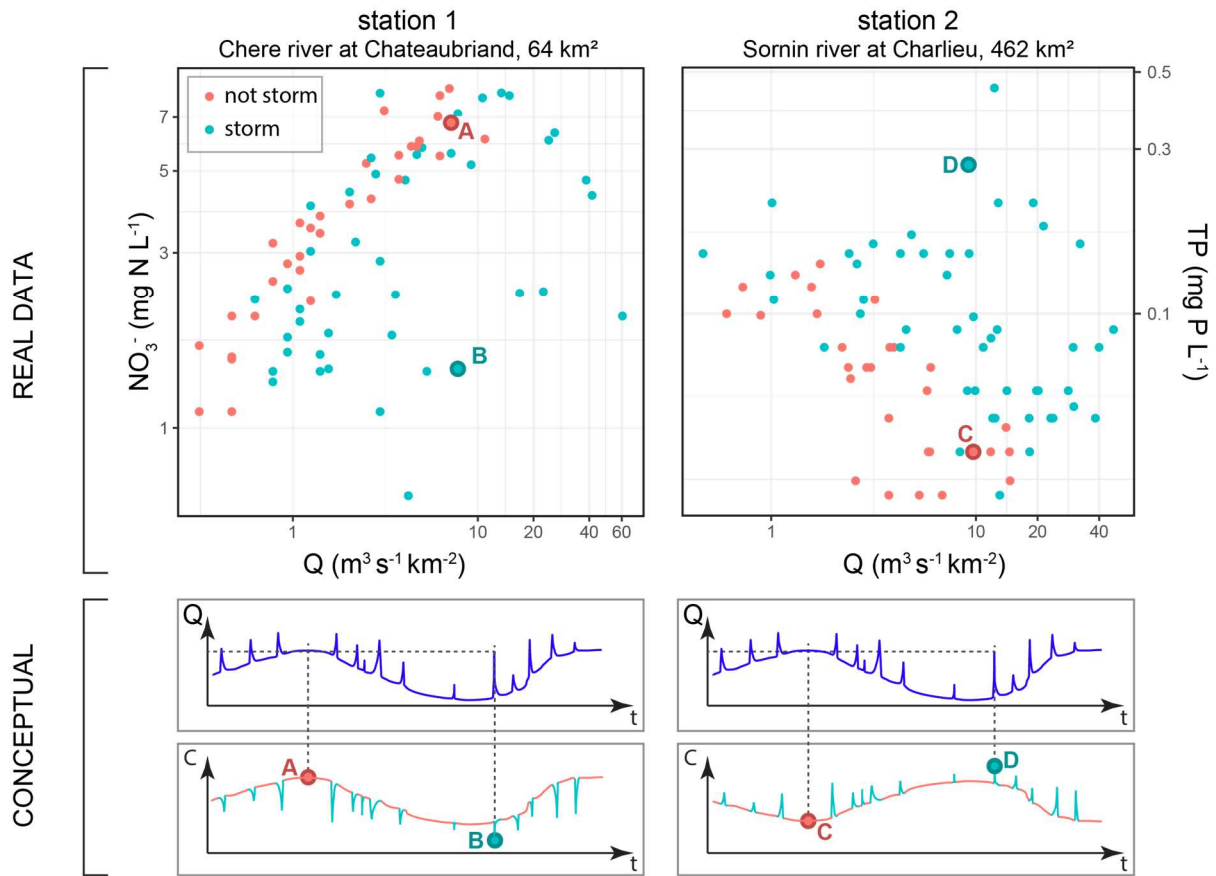
38 1. Introduction

39 The analysis of concentration-discharge (C-Q) relationships provides useful information on
40 the processes controlling the mobilization and delivery of chemical elements into streams (i.e.
41 export regimes) as well as biogeochemical transformations in river networks (Bieroza et al.,
42 2018; Godsey et al., 2009; Moatar et al., 2017; Musolff et al., 2017, 2015). Export regimes
43 have been classified as chemostatic, when concentrations vary little compared to discharge, or
44 chemodynamic, when concentrations variability is larger (Musolff et al., 2015). Export
45 regimes have generally been interpreted in terms of spatial distribution of sources in three
46 spatial dimensions: vertically in depth (Abbott et al., 2018; Dupas et al., 2016; Musolff et al.,
47 2016), laterally along hillslopes (Musolff et al., 2017) and longitudinally from upstream to
48 downstream reaches (Dupas et al., 2019a, 2017; Tiwari et al., 2017). Homogeneously
49 distributed sources mainly lead to chemostatic export regimes whereas heterogeneously
50 distributed sources mainly lead to chemodynamic export regimes (Basu et al., 2011; Dupas et
51 al., 2016; Godsey et al., 2009; Moatar et al., 2017; Musolff et al., 2015). Temporally variable
52 biogeochemical reactions in terrestrial and aquatic ecosystems may also enhance or attenuate
53 the chemostatic and chemodynamic character of export regimes (Minaudo et al., 2015).

54 Different metrics and thresholds have been used to characterize export regimes. On the one
55 hand, several authors have compared the coefficient of variation of concentration (CVC) to the
56 coefficient of variation of discharge (CVq) (Dupas et al., 2019b; Musolff et al., 2017, 2015;
57 Thompson et al., 2011; Underwood et al., 2017) or investigated the so-called “temporal
58 Lorenz inequality” (Gini coefficients, Jawitz & Mitchell, 2011; Williams et al., 2016). On the
59 other hand, other authors have used the slope of C-Q relationships in logarithmic domain as a
60 metric of export regimes: if the slope coefficient is non-significantly different from zero, the
61 export regime is considered chemostatic, while slopes significantly different from zero
62 characterize a chemodynamic export regime (Ameli et al., 2017; Basu et al., 2011; Diamond
63 and Cohen, 2018; Godsey et al., 2009; Kim et al., 2017; Koenig et al., 2017; Moatar et al.,
64 2017). This second approach allows not only to characterize export regimes as chemostatic
65 and chemodynamic, but also to describe observed patterns as dilution, constant and
66 mobilization archetypes (Musolff et al 2017). However, fitting a single linear regression on C-
67 Q plots is sometimes questionable due to large dispersion in C-Q plots (even log
68 transformed). Many factors cause this dispersion: i) hysteresis and non-linearity effects due to
69 source and transport limitations (Benettin et al., 2017); ii) instream biogeochemical
70 transformations on nutrient concentration without temporal correlation with hydrological
71 variations (Bieroza and Heathwaite, 2015; Moatar et al., 2017); iii) seasonal and long-term
72 variations in C-Q relationships (Hirsch, 2014; Zhang et al., 2016).

73 This dispersion in C-Q plots is a manifestation of ambivalent situations where the same Q
74 corresponds to different ecohydrological conditions in the catchment, and thus produces
75 different C (Bol et al., 2018). Ambivalent situations have been highlighted by several authors
76 who found opposite C-Q patterns (dilution versus mobilization) at seasonal and storm event
77 time scales (Duncan et al., 2017a; Dupas et al., 2017; Li et al., 2019) possibly leading to zero
78 C-Q slopes on average although both seasonal and storm event slopes were significantly
79 different from zero. Figure 1 is an illustrative example showing two C-Q relationships subject
80 to high dispersion effects. In these examples, discharge during a summer storm event is
81 comparable with discharge during winter baseflow, but ecohydrological conditions differ
82 considerably, leading to different concentrations. Nitrate tended to be highest during winter

83 baseflow (observation A), whereas P tended to be highest during a summer storm event
 84 (observation D). These examples suggest that considering both slow and quick flow
 85 components has the potential to improve C-Q models, and this is the main hypothesis of this
 86 paper.



87
 88 **Figure 1.** Concentration response to discharge fluctuations highly depends on the hydrological conditions (not only the value
 89 of discharge but also whether discharge is subjected to quick or slow variations). Top row: C-Q relationships at two stations
 90 located in France (left: nitrate, right: total phosphorus). Measurements during storm events were differentiated from the rest
 91 of the observations based on hydrograph separation (see section Method for details and data sources). Bottom row:
 92 Hypothetical responses of C to seasonal and storm event Q variations.

93 These examples also show that C observations during storm events overlap with values
 94 measured during baseflow periods. Therefore, splitting the C-Q diagram based on a percentile
 95 of discharge (Diamond and Cohen, 2018; Moatar et al., 2017) does not necessarily separate
 96 storm events from seasonal variations, and cannot possibly solve the dispersion effect
 97 commonly observed in C-Q plots. The approach developed in the WRTDS model (Weighted
 98 Regression on Time, Discharge and Season, Hirsch, 2014; Zhang et al., 2015; Zhang,
 99 Harman, et al., 2016; Zhang & Ball, 2017) addresses most of the dispersion issues listed
 100 above, and efficiently interpolates low-frequency time series. Unfortunately, the WRTDS
 101 model includes four parameters and therefore cannot be considered a parsimonious approach.
 102 These coefficients are calibrated at each time step, which makes difficult to interpret what
 103 drives the heterogeneity often observed in terms of catchment behavior.

104 This guided us towards the formulation of a double C-Q relationship, the model named
 105 hereafter “C-Q_{quick-slow}”, which enables seasonal (slow) C-Q slopes to differ from storm event
 106 (quick) C-Q slopes. Firstly, we assessed the skills of our C-Q_{quick-slow} model to fit observations
 107 and characterize nutrient export regimes at both temporal scales. Secondly, we explored the

108 spatial variability of the different C-Q archetypes encountered across diverse physical and
109 ecological contexts. We expected variability in these C-Q relationships to be primarily
110 controlled by land use and hydrological flow paths. To test this hypothesis, we established
111 statistical links between a set of catchment descriptors (e.g. land use cover, and
112 morphological, hydrological and geological attributes) and the C- $Q_{\text{quick-slow}}$ model parameters.
113 This was achieved using a large database comprising 219 independent catchments (11 to 2500
114 km²) where nitrate, total phosphorus and soluble reactive phosphorus concentrations have
115 been monitored monthly, and discharge measured daily, within a French national program for
116 water quality monitoring over the period 2008-2015.

117

118 2. Material and methods

119 2.1. C-Q analysis

120 We assumed that C-Q relationships are the combination of the C response to seasonal (slow)
121 Q variations with the C response to storm-event (quick) Q variations, and this constituted the
122 essence of the “C- $Q_{\text{quick-slow}}$ ” model. It does not necessarily mean that Q variations are the
123 cause of C variations, but only that they covary or anti-covary in time. The seasonal and storm
124 event variations in discharge were estimated from hydrograph separation into slow and quick
125 components (Equation 1).

$$126 \quad C(t) = \beta_0 + \beta_1 \cdot \log(Q_{\text{slow}}(t)) + \beta_2 \cdot \log(Q_{\text{quick}}(t)) + \varepsilon \quad \text{Equation 1}$$

127 where all β_i are adjusted coefficients, and ε represents the residuals.

128 To estimate Q_{slow} and Q_{quick} , we normalized discharge by interannual median flow, and used
129 the baseflow recursive filter method (Lyne and Hollick, 1979; Nathan and McMahon, 1990)
130 with 3 passes and a filter parameter set at 0.925. This method separates total flow into a
131 seasonal component and a short-term component called hereafter “storm event” in the
132 manuscript. Seasonality of the “slow” component was verified by computing autocorrelation
133 curves of Q_{slow} at all sites (Figure S.1 in Supplement file).

134 Model outputs consisted in the fitted coefficients $\beta_0, \beta_1, \beta_2$ and performance indicators: the
135 root mean squared error normalized by the standard deviation of observations ($nRMSE$),
136 adjusted explained variance (R^2_{adj}), and p-values for each coefficient in Equation 1. A
137 linearity test was computed on residuals to verify that 95% of studentized residuals lied within
138 the interval [-2, 2].

139 For both the seasonal and the storm event scales, the relationship between C and Q variations
140 could either be positive (covariation, or mobilization), negative (anti-covariation, or dilution)
141 or non-significant (chemostasis for nearly constant C, or neutrality when C variations exist
142 that are not driven by Q fluctuations). We considered a relationship to be non-significant
143 when the associated p-value exceeded 0.05. The sign of the C-Q relationship at the seasonal
144 scale (β_1) could be different from the sign of the C-Q relationship at the storm event scale
145 (β_2). Thus, three possibilities (negative, non-significant, and positive) for two temporal scales
146 (slow and quick) led to consider that only 9 different C-Q archetypes theoretically exist.

147 2.2. Dataset for C-Q analysis

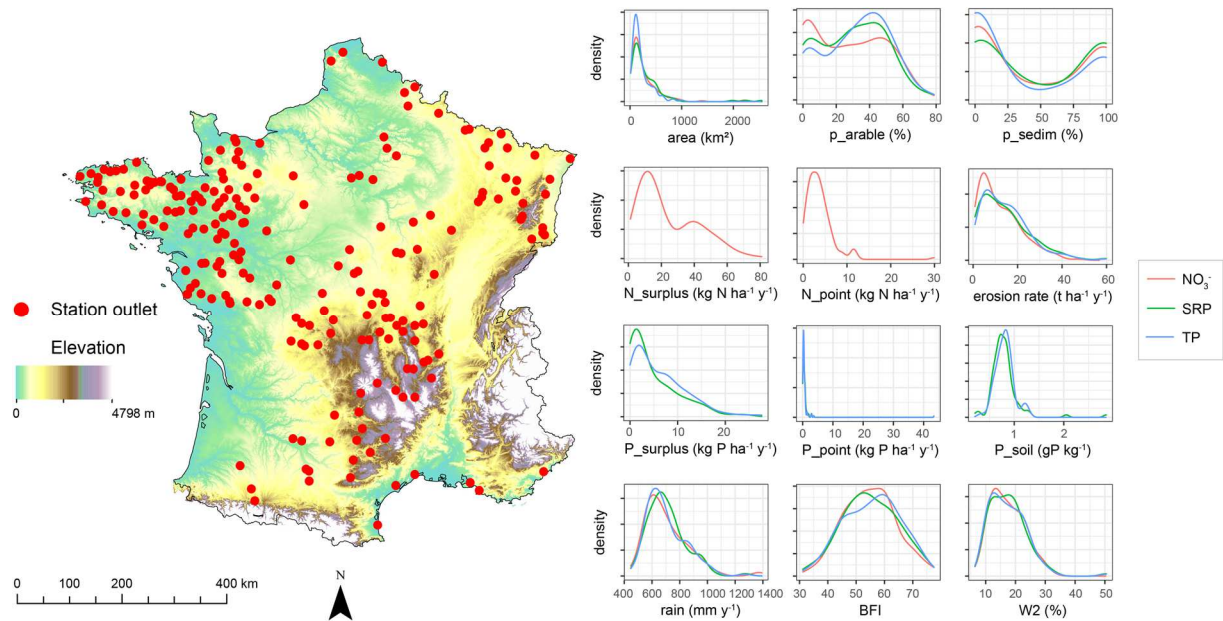
148 Water quality parameters included in this analysis were nitrate (NO_3^-), total phosphorus (TP)
149 and soluble reactive phosphorus (SRP). Concentrations were measured on grab samples
150 collected for physico-chemical analysis every other month on average. Across approximately
151 10,000 water quality stations present in the French national public database
152 (<http://www.naiades.eaufrance.fr/>), we selected stations meeting all the following criteria: i) C
153 station can be paired with a Q station (data from <http://www.hydro.eaufrance.fr/>) when their
154 catchments share at least 90% surface area; ii) all C catchments are independent; iii) C data
155 contains at least 50 observations after outliers removal (i.e. values over 200 mgN L^{-1} and 5 gP
156 L^{-1}) over the period 2008-2015; iv) at least 30% of C observations occurred during “major”
157 hydrological events (defined here as $Q(t) > 1.5 \times Q_{slow}$); v) trends on C are non-significant
158 over the period (p-value of Sen’s Slope test > 0.05 , following Hipel and McLeod (2005)) to
159 avoid penalizing the model. Finally, stations where a single concentration value was observed
160 more than 15% of the time were removed from the selection, a situation often seen in P
161 surveys when concentrations are below quantification limits. This resulted in 219 catchments
162 with respectively 179, 138 and 107 individual time series for NO_3^- , TP and SRP.

163 2.3. Relationships with catchment descriptors

164 The selected catchments encompassed contrasting physical contexts in terms of morphology,
165 nutrient diffuse and point sources, and hydrological and geological properties (see Table 1
166 and Figure 2 for data description). Catchment size ranged from 11 to 2500 km^2 , with 87% of
167 catchments $< 500 \text{ km}^2$. Approximately 55% of the catchments had at least 1/3 of their total
168 area covered by arable land (p_{arable}), indicating potentially high N and P surplus and thus
169 stream water quality likely to be significantly impacted by diffuse agricultural sources. Most
170 catchments received limited N and P point sources (only 10% received over $10 \text{ kg N ha}^{-1} \text{ y}^{-1}$,
171 and only 2% received over $0.1 \text{ kg P ha}^{-1} \text{ y}^{-1}$). Lithological contexts included both sedimentary
172 and crystalline bedrocks dominancy as shown by bimodal density plot on the percentage of
173 catchment over a sedimentary bedrock (p_{sedim} on Figure 2). Hydrological descriptors
174 covered a large climatic gradient: mean \pm standard deviation of effective rainfall, base flow
175 index (BFI) and index of hydrological reactivity (W2) (descriptions in Table 1) were
176 respectively $700 \pm 160 \text{ mm y}^{-1}$, 55 ± 9 and $17 \pm 5\%$.

177 We investigated the link between fitted coefficients of the fitted C- $Q_{quick-slow}$ model with a set
178 of catchment descriptors (Table 1 and Figure 2), using Pearson correlation coefficients
179 (assuming linear relationships) and associated p-values. We considered correlations as
180 significant when p-value < 0.05 . We conducted this correlation analysis on a subset of C-Q
181 fitted coefficients that exhibited reasonable goodness of fit ($nRMSE < 200\%$).

182



183

184 **Figure 2.** Monitoring stations for analysis and density plots of their catchment descriptors (see Table 1 for descriptors’
 185 definitions).

186

187 **Table 1.** List of catchment descriptors included in the analysis, and associated sources.

Descriptor type	Variable name	Unit	Definition	Source
Morphology	area	km ²	Catchment area	http://www.naiades.eaufrance.fr/
Diffuse and point N and P sources	N_surplus	kg N ha ⁻¹ y ⁻¹	Surplus of nitrogen and phosphorus	NOPOLU model. Doublet & Le Gall (2013); Snoubra (2013); (Dupas et al., 2015a) http://assainissement.developpement-durable.gouv.fr/services.php http://www.eau-loire-bretagne.fr/informations_et_donnees
	P_surplus	kg P ha ⁻¹ y ⁻¹		
	N_point	kg N ha ⁻¹ y ⁻¹	Nitrogen and phosphorus loads of domestic and industrial point sources	
	P_point	kg P ha ⁻¹ y ⁻¹		
	P_soil	g P kg ⁻¹	Total phosphorus soil content	Delmas et al., (2015)
Soil erosion	erosion	t ha ⁻¹ y ⁻¹	Erosion rate derived from land use, topography and soil properties	Cerdan et al., (2010)
Hydrological indicators	precipitation	mm y ⁻¹	Average effective rainfall, calculated as P-ETP for the months when P-ETP > 0	SAFRAN database, Quintana-Segui et al., (2008)
	BFI	-	Base flow index Index of hydrological reactivity representing the percentage of total discharge that occurs during the highest 2% flows	Eckhardt (2008)
	W2	%		Moatar et al., (2013)
Land use	p_arable	%	Percentage of arable land	Corine Land Cover (2006)
Geology	p_sedim	%	Percentage of sedimentary rocks derived from simple lithological maps	LITHO database (2008)

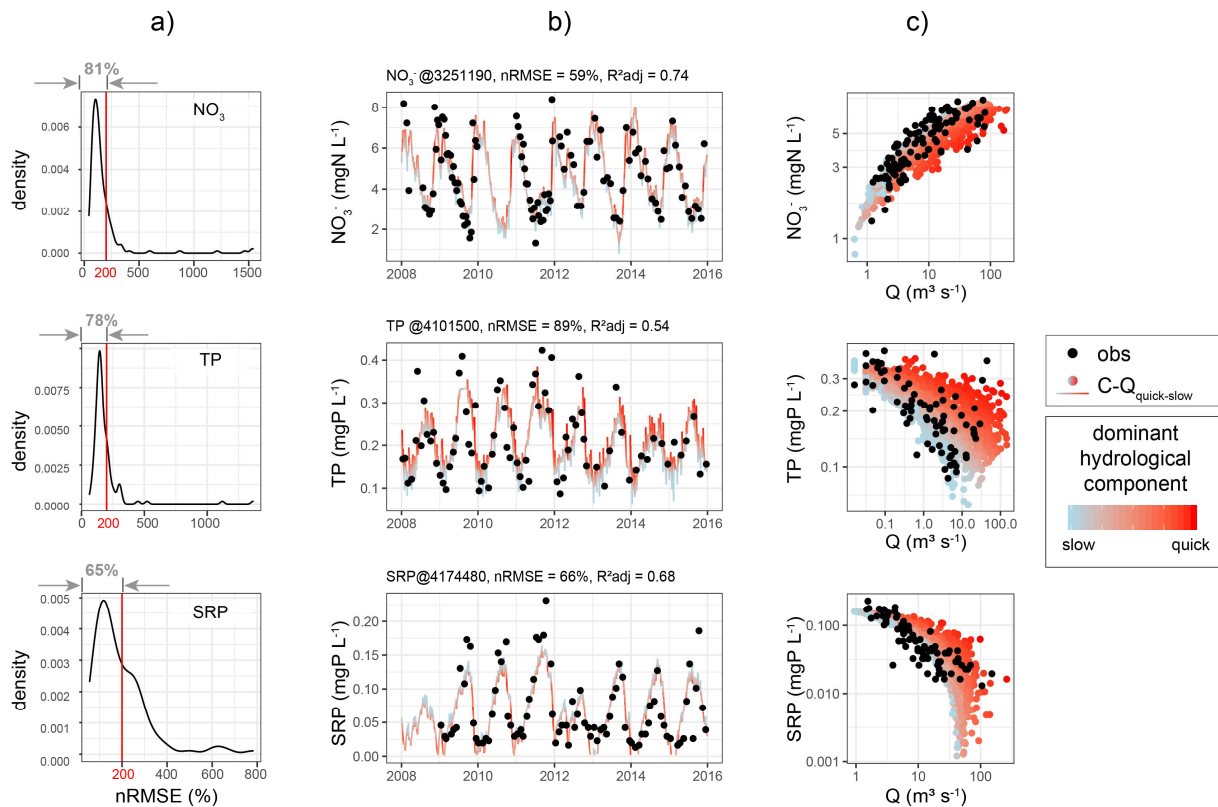
188

189 All analyses were conducted with R (R Core Team, 2016) with ‘EcoHydRology’, ‘lubridate’,
 190 ‘hydroGOF’, ‘trend’, ‘GGally’ and ‘ggplot2’ packages.

191 3. Results

192 3.1. C-Q model performances

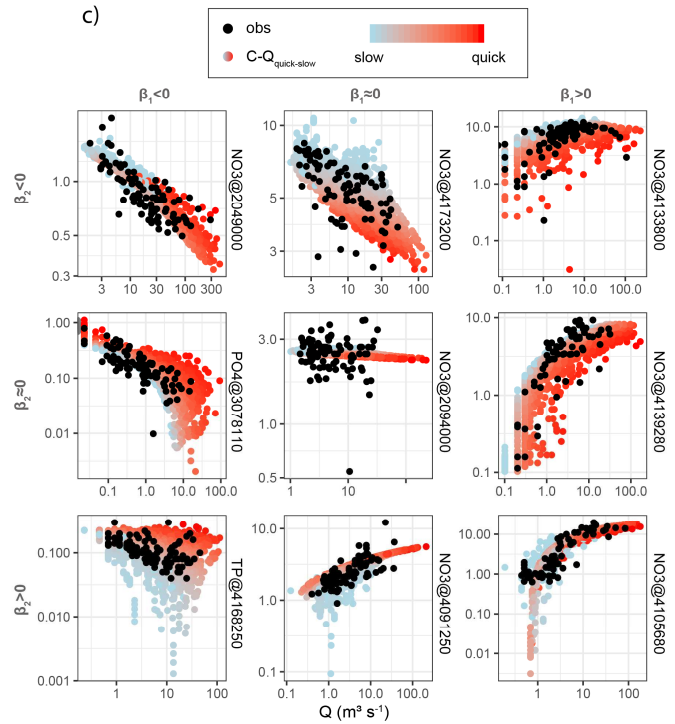
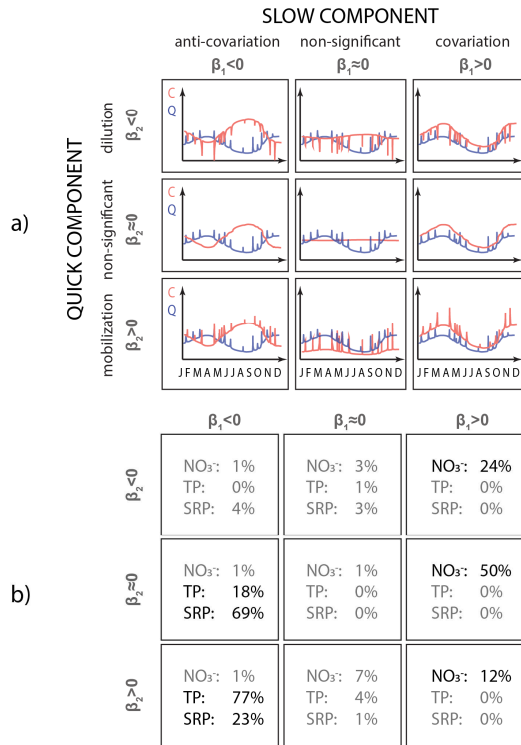
193 The *nRMSE* was under 200%, for 81%, 78% and 65 % of catchments for NO_3^- , TP and SRP,
 194 respectively (Figure 3). The median R^2_{adj} value was 0.39, 0.28 and 0.30 for NO_3^- , TP and
 195 SRP, respectively, and 10th percentile – 90th percentile ranges of R^2_{adj} were 0.12-0.63, 0.11-
 196 0.43, and 0.07-0.60. Approximately 80% of model fits passed the linearity test (results not
 197 shown). In the examples of Figure 3, seasonal variations were well reproduced, and
 198 concentration dynamics during short term storm events seemed to be correctly modeled for
 199 both dilution and mobilization processes, even if some storm events were sometimes
 200 underestimated. C-Q behaviors in a logscale C-Q diagram showed contrasting patterns, and
 201 dispersion in these plots varied depending on which component (slow or quick) dominated the
 202 total flow.



203 **Figure 3.** a) C-Q fits performances (*nRMSE* density plots) at all stations. Red vertical lines indicate *nRMSE* =200%. Grey
 204 percentages above density plots indicate the proportion of stations with *nRMSE* under 200%.; b) examples of C-Q fits for
 205 NO_3^- , TP and SRP at three different stations and c) depicts the same observed and modelled concentrations in more classical
 206 logscale C-Q plots.

208 3.2 C-Q typologies for N and P

209 Interestingly, only 2 or 3 C-Q archetypes among the nine possibilities were observed for each
 210 parameter (Figure 4). For NO_3^- , the seasonal component covaried positively in most cases
 211 with baseflow seasonality ($\beta_1 > 0$ for 86% of the catchments), and the dynamics during storm
 212 were either non-significant (52% cases), showing a dilution pattern ($\beta_2 < 0$, 28% of cases), or
 213 a mobilization pattern ($\beta_2 > 0$, 20%). Thus, the most represented archetype was a positive C-Q
 214 slope at the seasonal scale combined with a non-significant storm component (50% cases).



215

216 **Figure 4.** a) conceptual daily evolutions over one year for C and Q based on the nine potential C-Q archetypes, b)
 217 proportions of C-Q archetypes encountered in our database for NO₃⁻, TP and SRP for catchments where $nRMSE < 200\%$.
 218 Numbers in black highlight archetypes encountered in more than 10% occurrences, and c) examples of logscale C-Q plots for
 219 each of these 9 possibilities.

220 For TP, 95% of catchments displayed seasonal variations opposite to baseflow seasonality (β_1
 221 < 0). The remaining 5% presented a non-significant seasonal component. The TP dynamics
 222 during storm events were a mobilization pattern in most cases ($\beta_2 > 0$ for 81%), and the
 223 remaining 19% presented non-significant dynamics during storms. The most represented C-Q
 224 archetype for TP was a negative C-Q slope at the seasonal scale, combined with a
 225 mobilization storm component (77%). For SRP, seasonality was similar to TP, i.e. a negative
 226 C-Q slope at the seasonal scale for 96% of the catchments ($\beta_1 < 0$). Compared to TP, a larger
 227 proportion of catchments presented a non-significant storm event component. This concerned
 228 69% catchments and represented the most observed C-Q archetype as 23% presented a
 229 mobilization pattern and only 4% a dilution pattern.

230 These nine different C-Q archetypes were highly contrasted when presented in a classic
 231 logscale C-Q diagram (Figure 4c). Dilution or mobilization patterns were clearly represented
 232 and dispersion in the plots depended on which component (slow or quick) dominated. Points
 233 corresponding to a quick component dominating the total flow were found on top or bottom of
 234 the cloud of points depending on the sign of β_2 . As expected from our C-Q model design,
 235 negative β_2 produced a larger dispersion towards lower C values, and positive β_2 produced a
 236 larger dispersion towards higher C values.

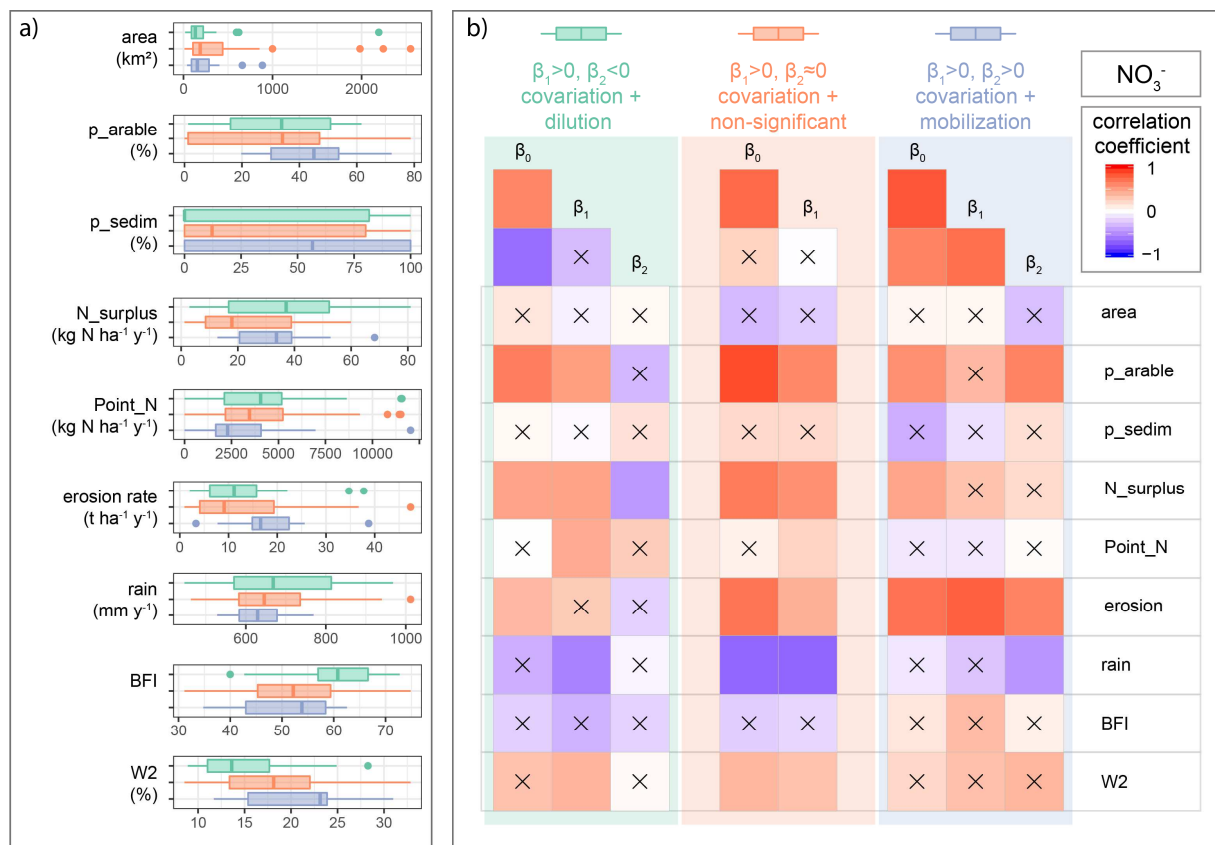
237

238 3.2. Linking C-Q relationships with catchment descriptors

239 The link between C-Q fitted coefficients calibrated with Equation 1 and a set of catchment
 240 descriptors was assessed based on linear Pearson correlations. We computed correlation
 241 values for the C-Q types encountered more than 10% of the time in the database (section 3.1).

242 The coefficient β_0 represented the background pollution, β_1 was associated with seasonal
 243 variations, and β_2 the variations in storms.

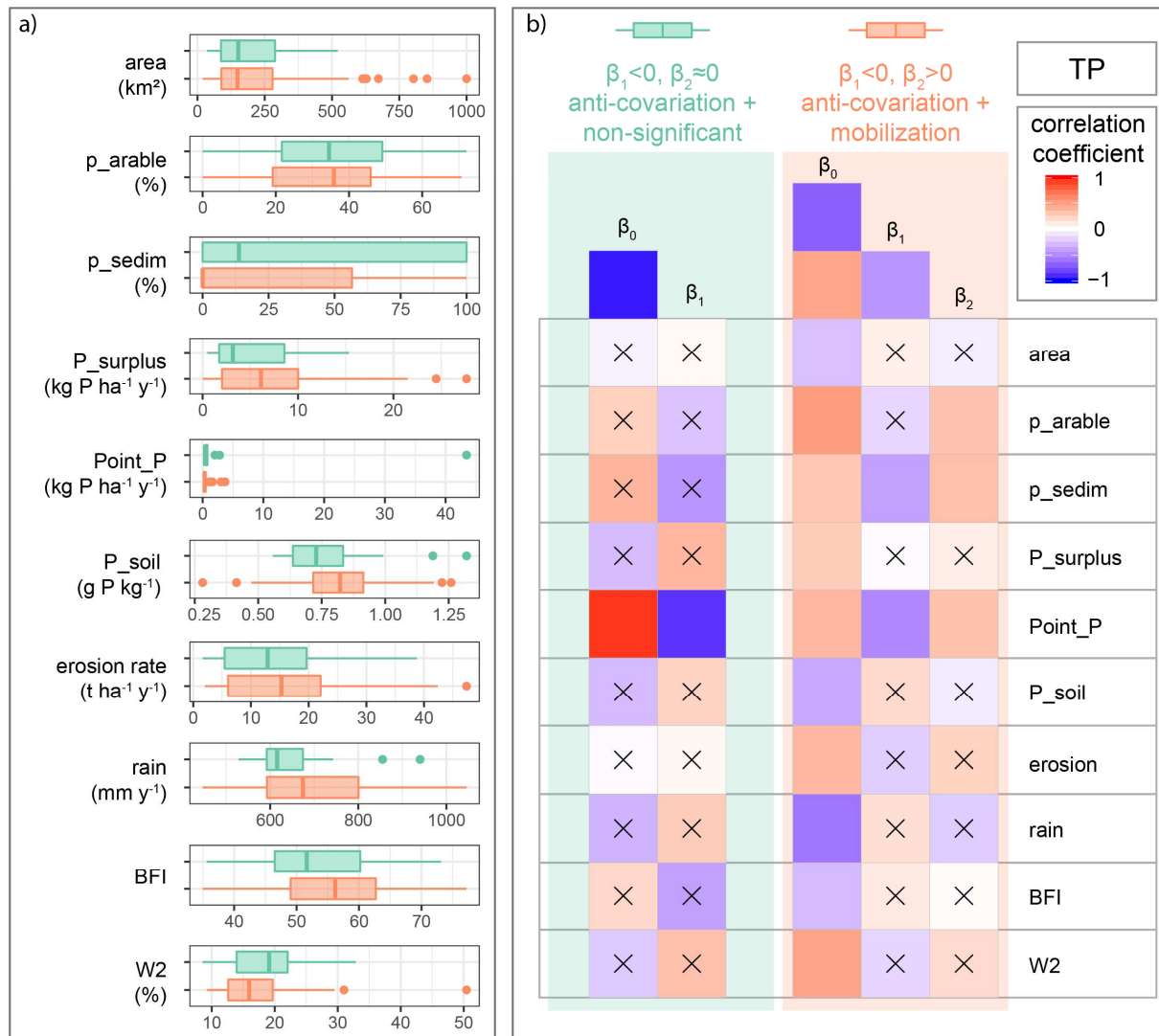
244 For NO_3^- (Figure 5), the background pollution β_0 was highly correlated with diffuse
 245 agricultural sources (R correlation coefficients ranged from 0.6 to 1 with N surplus and the
 246 proportion of arable land in the catchment) for all C-Q types identified. The seasonal
 247 component β_1 was highly linked with β_0 (correlation was over 0.9), indicating larger seasonal
 248 magnitude in the most polluted catchments. The magnitude of the storm component β_2 was
 249 linked to diffuse sources: significant correlation coefficients were found between β_2 and
 250 p_arable, N surplus, and erosion rate depending on the C-Q type. Hydrological descriptors,
 251 erosion rate and lithology classes differentiated the catchments presenting contrasting C-Q
 252 archetypes: dilution patterns in storms ($\beta_2 < 0$) were associated with high BFI values, low W2
 253 values, low values of erosion rate and mostly located on crystalline bedrock. By contrast,
 254 mobilization patterns in storms ($\beta_2 > 0$) were associated with catchments presenting low BFI,
 255 high W2 and high erosion rate, and mostly located on sedimentary rocks.



256
 257 **Figure 5.** Ranges (a) and correlation matrices (b) between C-Q features (selection based on nRMSE < 200%) characterized
 258 by NO_3^- background pollution (β_0), seasonal C-Q (β_1), storm C-Q (β_2) and catchment descriptors for the most represented
 259 NO_3^- -Q types (more than 10% occurrences). Black crosses indicate non-significant correlations. Pearson correlation
 260 coefficients among catchment descriptors can be found in Table S.1 in the Supplement file.

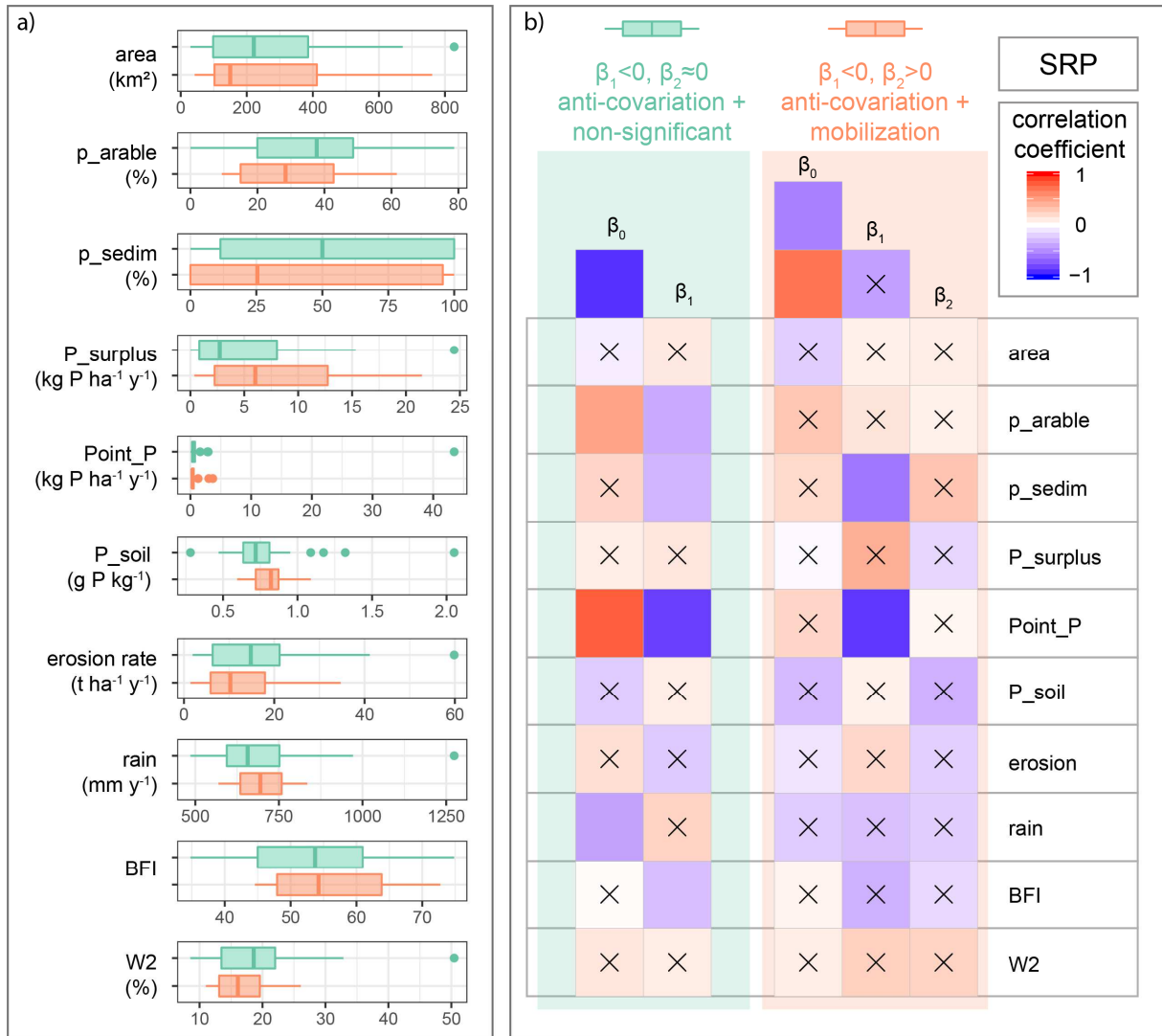
261 For TP (Figure 6), the coefficient β_0 was highly and positively correlated with point P sources
 262 (R was 0.6 to 1). Seasonal dynamic was always opposite to the baseflow Q seasonality ($\beta_1 < 0$)
 263 (Figure 4). The amplitude of the seasonal component β_1 was clearly anti-correlated with P
 264 point sources (R was -1 to -0.8). We found that, compared to catchments where behavior in
 265 storms was not significant, catchments with significant mobilization storm event component
 266 presented higher ranges of P surplus, soil P content, erosion rate, effective rainfall, and BFI

267 and lower range of W2. In the case of significant mobilization pattern during storm events, the
 268 highest correlations with β_2 were found with P point sources (R was 0.7). In the case of
 269 significant mobilization pattern during storm events, rainfall, BFI and W2 presented strong
 270 correlations with β_0 (R were respectively -0.9, -0.6 and 0.7).



271
 272 **Figure 6.** Ranges (a) and correlation matrices (b) between C-Q features (selection based on nRMSE < 200%) characterized
 273 by TP background pollution (β_0), seasonal C-Q (β_1), storm C-Q (β_2) and catchment descriptors for the most represented TP-Q
 274 types. Black crosses indicate non-significant correlations. Pearson correlation coefficients among catchment descriptors can
 275 be found in Table S.1 in the Supplement file.

276 For SRP (Figure 7), although correlations between SRP C-Q coefficients and catchment
 277 descriptors were lower or less significant than the correlation found for the analysis on TP,
 278 similar interpretation could be made: β_0 and β_2 were positively linked with point sources,
 279 while seasonality β_1 was anti-correlated with point sources. Compared to catchments with a
 280 non-significant storm component, catchments with mobilization storm event components
 281 presented higher ranges of P surplus, soil P content, and lower erosion rate.



282
 283 **Figure 7.** Ranges (a) and correlation matrices (b) between C-Q features (selection based on nRMSE < 200%) characterized
 284 by SRP background pollution (β_0), seasonal C-Q (β_1), storm C-Q (β_2) and catchment descriptors for the most represented
 285 SRP-Q types. Black crosses indicate non-significant correlations. Pearson correlation coefficients among catchment
 286 descriptors can be found in Table S.1 in the Supplement file.

287 **4. Discussion**

288 **4.1. Nutrient export regimes at seasonal and storm event scales**

289 The C-Q_{quick-slow} model revealed different export regimes for nitrate and phosphorus forms at
 290 both seasonal and storm event time scales. Nutrient concentration responses to storm events
 291 were sometimes opposite to seasonal responses to Q variations, resulting in large dispersion in
 292 C-Q plots as is usually observed. This supports the observations from previous studies
 293 (Duncan et al., 2017b, 2017a; Li et al., 2019) showing that C-Q relationships may vary across
 294 different time scales because the different processes shaping C-Q curves have different
 295 temporalities.

296 Despite the diversity of catchment characteristics in our analysis, only two or three C-Q
 297 archetypes were observed among nine theoretical possibilities. This supports the idea
 298 developed in Moatar et al. (2017) that the same processes control respectively N and P
 299 transfers, across a wide range of environmental conditions.

300 Seasonal variations displayed consistent patterns across the entire database: we observed
301 positive slow component for nitrate ($\beta_1 > 0$), and negative slow component for phosphorus
302 ($\beta_1 < 0$). The processes responsible for seasonal covariation between nitrate and baseflow are
303 either associated with connectivity fluctuation between the stream and the groundwater table
304 (Curie et al., 2011; Duncan et al., 2015; Pinay et al., 1993), or with riparian and in-stream
305 denitrification and biological assimilation (uptake). Disentangling these different processes is
306 challenging because they often occur at the same time: biogeochemical transformations often
307 take place in conditions with high temperature and/or light conditions and long residence
308 times, which coincides with periods of low hydrological connectivity and thus low transport
309 capacity. Opposite seasonality variations between phosphorus concentration and discharge
310 probably result from point sources and their degree of dilution controlling seasonal variations.
311 However, recent studies have found that summer reductive dissolution of iron oxy-hydroxide
312 could also mimic this point-source signal (Dupas et al., 2018; Smolders et al., 2017). It is
313 however noteworthy to remind that in large eutrophic rivers, SRP seasonality can covary with
314 baseflow seasonality due to large algae uptake when low flow coincides with long transit
315 time, optimal light, and temperature conditions (Minaudo et al., 2018, 2015). This particular
316 pattern was not observed in the present study, and we would argue that the selected
317 catchments were too small for algal uptake to become a dominant driver of SRP seasonality.

318 Storm components for nitrate were in most cases non-significant, suggesting almost unlimited
319 N supply due to large legacy effects (Van Meter and Basu, 2015). This storm component was
320 sometimes negative, indicating dilution effects of diffuse sources by overland flow (Dupas et
321 al., 2016; Fovet et al., 2018). The storm component was sometimes positive, indicating a
322 temporary reconnection between surface and sub-surface waters in catchments likely
323 presenting a vertical gradient of N sources: storms likely flush N stored in the vadose zone
324 (Bende-Michl et al., 2013). For P, when significant, the storm component was in most cases
325 positive, indicating the mobilization of both particulate and dissolved phosphorus. This may
326 occur near agricultural areas with potential interactions with sub-surface water (Dupas et al.,
327 2015c; Gu et al., 2018, 2017; Minaudo et al., 2017), or in-stream by simply re-mobilizing fine
328 sediments stored in the river bed or stored in the river banks (Jarvie et al., 2012; Powers et al.,
329 2016).

330

331 4.2. What determines C-Q relationships at the seasonal and storm event scales?

332 Other studies have looked at potential links between C-Q parameters and catchment
333 descriptors. In most cases, correlations were poor (Diamond and Cohen, 2018; Godsey et al.,
334 2009) but these works evidenced relationships with catchment size, land use, and lithology. In
335 our study, and for all three NO_3^- , TP and SRP, we found strong correlations between C-Q
336 coefficients β_i and readily available catchment variables derived from open-access GIS
337 databases. We found that the magnitude of the background pollution β_0 is determined by
338 diffuse sources intensity (N surplus or p_{arable}) for nitrate, and by point-sources inputs
339 (P_{point}) for TP and SRP. Interestingly, and for all three parameters, the absolute magnitude
340 of the seasonal component β_1 was positively correlated with higher background pollution
341 concentration β_0 , suggesting that diffuse sources and point sources respectively control
342 seasonal amplitudes of nitrate and phosphorus concentrations. This implies that the most
343 polluted catchments are also the ones with the highest seasonal amplitudes. Different reasons

344 can explain this observation. For nitrate, baseflow concentrations during winter high flow
345 varied more than during summer low flow among the catchments (see Supplementary Figure
346 S.2) arguably because stoichiometric controls during the summer period lead to similar
347 concentrations in different types of catchments, whereas winter concentration better reflects N
348 sources intensity among catchments (Fovet et al., 2018). This supports some recent findings
349 showing that spatial stability for nitrate concentrations is higher over winter months (Dupas et
350 al., 2019b). For phosphorus, we showed that point sources largely control the background
351 pollution in the catchments studied here. Thus, higher loads discharged constantly throughout
352 the year in rivers where flow variations are seasonal is likely to result in limited dilution
353 capacity during low flows, producing large seasonal variations in concentrations

354 During storm events, we found that the dynamics of both nitrate and phosphorus were linked
355 to both nutrient source indicators and hydrological properties. For instance, we found for NO_3^-
356 that high BFI values, low W2, and low erosion differentiated C-Q dilution patterns from non-
357 significant and mobilization types. This suggested that catchments where shallow
358 groundwater flow contribution dominates are likely to display dilution patterns in storm
359 events due to a sudden increased contribution of young age water (Benettin et al., 2017;
360 Hrachowitz et al., 2016). For TP and SRP, we found that wet catchments with high diffuse P
361 sources and high erosion rates were likely to display a significant mobilization storm event
362 component. This supported the idea that dissolved and particulate P flush during a short term
363 storm event is the consequence of re-mobilization of particles from the river bed or from the
364 streams bank sides (Fox et al., 2016), or the result of an increased connectivity between
365 groundwater and streamflow (Ali et al., 2017; Dupas et al., 2015c; Gu et al., 2017; Rose et al.,
366 2018).

367 4.3. Potential use of this approach for load estimations

368 In most countries, water quality monitoring strategies rely on low frequency surveys, typically
369 executed monthly (Dupas et al., 2019b). These surveys are used to determine the water quality
370 status of streams based on a set of simple metrics such as the interannual 90th percentile
371 concentration or interannual fluxes. The validity of these estimations derived from low
372 frequency data has largely been questioned (e.g. Audet et al., 2014; Cassidy and Jordan, 2011;
373 Johnes, 2007; Moatar et al., 2013; Raymond et al., 2013; Rozemeijer et al., 2010), and raises
374 some major management issues where the assessment of water quality indicators is critical.
375 When applicable, the C- $Q_{\text{quick-slow}}$ model has the potential for interpolating low frequency C
376 time series based on daily Q, and therefor decreases uncertainties in water quality indicators.
377 We illustrated this potential with data from one water quality station located in Brittany where
378 nitrate was monitored daily between 2007 and 2011 (See supplement file). First we
379 subsampled the data to simulate a monthly survey, and then interpolated the subsampled data
380 using the C- $Q_{\text{quick-slow}}$ model and compared the reconstructed daily concentration and loads to
381 the observations. Results with this example were promising: NO_3^- annual load errors remained
382 under 5% (instead of 10% with a discharge weighted method commonly used in the literature
383 (Moatar and Meybeck, 2005)) and average \pm standard deviation errors on monthly loads were
384 $8 \pm 6\%$.

385 Additionally, the high correlations observed between C-Q coefficients and catchment
386 descriptors suggest that it is possible to predict the most likely C-Q archetype for any
387 catchment, and, then estimate annual and seasonal loads. Applications are numerous and

388 might be the key to empirical estimation of loads in catchments where discharge is measured
389 or can be modelled, but not water quality. Predicting C-Q relationships based on our
390 formulation has to be tested on a large database that covers a large diversity of local contexts
391 in terms of catchment morphology, geology, land use, climate and hydrology.

392 4.4. Limits and perspectives

393 Although the C-Q_{quick-slow} model provided good results for a majority of catchments, C-Q fits
394 were poor for another significant proportion of them. This failure to fit the C-Q_{quick-slow} model
395 to these catchments means that they do not match one or several of the hypothesis of the
396 model: they could display more complex patterns than what the model can describe, or be too
397 chemostatic for a C-Q model to perform well. For example, the C-Q_{quick-slow} model does not
398 consider hysteresis effects at both seasonal and storm event times scales, although these are
399 commonly observed (Bieroza and Heathwaite, 2015; Dupas et al., 2015b; Minaudo et al.,
400 2017; Rose et al., 2018). Besides, the slow and quick components defined based on baseflow
401 separation techniques represent in reality more a separation of responses in time to streamflow
402 variations than a water source separation (McDonnell and Beven, 2014). In the particular case
403 of nitrate, we assumed that a concentration gradient across the subsurface-to-groundwater
404 layer would be enough to explain slow and quick variations in time, but a non-significant
405 quick component in 52% cases in our study may indicate a conceptual limitation of our
406 model. Indeed, the C-Q_{quick-slow} model does not allow storm event responses to vary across
407 seasons, although several studies have documented these variations (Dupas et al., 2016; Fovet
408 et al., 2018). In our approach, the magnitude of C variations among events as a linear function
409 of log-transformed quickflow variations, but the sign of the C-Q coefficient β_2 or its intensity
410 across a succession of similar Q events could not change. Thus, the C-Q relationship could
411 only be poorly adjusted to the observations for catchments where the behavior for summer
412 storms is for instance inverted compared to the behavior for winter storms, or where C supply
413 is easily depleted. An interaction term between the two temporal scales could be added to the
414 equation, but this would result in an additional coefficient that would increase the risk of
415 overfitting the model. Finally, we assumed in this study that grab samples could represent a
416 daily mean concentration, which is not verified in several studies in small catchments
417 showing large sub-daily variations (Halliday et al., 2015; Minaudo et al., 2017; Rode et al.,
418 2016), thus increasing uncertainty of the model calibration data. Although this certainly limits
419 the use of the C-Q_{quick-slow} model with grab sample data in small and hydrologically reactive
420 catchments, the model could be tested with sub-daily probe data where they exist.

421 5. Conclusions

422 The C-Q_{quick-slow} model is a new C-Q model that considers the possibility for different C-Q
423 relationships at the storm event scale and at the seasonal scale. Results showed that the slopes
424 of C-Q relationships can be different or even opposite at storm event time and seasonal scales,
425 which explains a large part of the dispersion commonly observed in C-Q plots.

426 We showed that NO₃⁻-Q relationships at the seasonal scale were in 75% cases positive and
427 relationships in storms were either showing dilution pattern (24% cases), a non-significant
428 pattern (50%), or a mobilization pattern (12%). TP and SRP relationships with Q at the
429 seasonal scale were almost systematically negative (95%), and patterns during storm events
430 were in most cases showing a mobilization for TP (77%) or were non-significant for SRP
431 (69%). We have linked the different C-Q relationships with catchment descriptors and found

432 that indicators of diffuse sources loads determined NO_3^- seasonal amplitudes, and hydrological
433 drivers could explain the behavior during storms. In contrast, point sources determined P
434 seasonal amplitudes, and diffuse sources combined with erosion rate likely controlled P
435 behavior during storm events. The C- $Q_{\text{quick-slow}}$ model has the potential to improve nutrient
436 load estimations because of the good predictability of appropriate C-Q archetypes and the
437 possibility to interpolate low frequency concentration data to a daily frequency.

438

439 **Author contributions**

440 The concept for this paper emerged during discussions between C.M. and R.D. C.M.
441 downloaded the data and ran the GIS, model and statistical analysis. C.M. wrote the
442 manuscript with input from all the co-authors.

443

444 **Acknowledgements**

445 This work was funded by the “Agence Française pour la Biodiversité (AFB)”, the French
446 National Agency for Biodiversity. The authors are grateful to the French Water Basin
447 Agencies and their partners who contributed to the water quality data acquisition. Water
448 quality and discharge data used in this study are available from public repositories at
449 <http://osur.eau-loirebretagne.fr/> and <http://hydro.eaufrance.fr/>.

450

451

452 **References**

- 453 Abbott, B.W., Moatar, F., Gauthier, O., Fovet, O., Antoine, V., Ragueneau, O., 2018. Trends
454 and seasonality of river nutrients in agricultural catchments: 18 years of weekly citizen
455 science in France. *Sci. Total Environ.* 624, 845–858.
456 <https://doi.org/10.1016/j.scitotenv.2017.12.176>
- 457 Ali, G., Wilson, H., Elliott, J., Penner, A., Haque, A., Ross, C., Rabie, M., 2017. Phosphorus
458 export dynamics and hydrobiogeochemical controls across gradients of scale, topography
459 and human impact. *Hydrol. Process.* 31, 3130–3145. <https://doi.org/10.1002/hyp.11258>
- 460 Ameli, A.A., Beven, K., Erlandsson, M., Creed, I.F., McDonnell, J.J., Bishop, K., 2017.
461 Primary weathering rates, water transit times, and concentration-discharge relations: A
462 theoretical analysis for the critical zone. *Water Resour. Res.* 53, 942–960.
463 <https://doi.org/10.1002/2016WR019448>
- 464 Audet, J., Martinsen, L., Hasler, B., De Jonge, H., Karydi, E., Ovesen, N.B., Kronvang, B.,
465 2014. Comparison of sampling methodologies for nutrient monitoring in streams:
466 Uncertainties, costs and implications for mitigation. *Hydrol. Earth Syst. Sci.* 18, 4721–
467 4731. <https://doi.org/10.5194/hess-18-4721-2014>
- 468 Basu, N.B., Thompson, S.E., Rao, P.S.C., 2011. Hydrologic and biogeochemical functioning
469 of intensively managed catchments: A synthesis of top-down analyses. *Water Resour.*
470 *Res.* 47, n/a-n/a. <https://doi.org/10.1029/2011WR010800>
- 471 Bende-Michl, U., Verburg, K., Cresswell, H.P., 2013. High-frequency nutrient monitoring to
472 infer seasonal patterns in catchment source availability, mobilisation and delivery.
473 *Environ. Monit. Assess.* 185, 9191–9219. <https://doi.org/10.1007/s10661-013-3246-8>
- 474 Benettin, P., Bailey, S.W., Rinaldo, A., Likens, G.E., McGuire, K.J., Botter, G., 2017. Young
475 runoff fractions control streamwater age and solute concentration dynamics. *Hydrol.*
476 *Process.* 31, 2982–2986. <https://doi.org/10.1002/hyp.11243>
- 477 Bieroza, M., Heathwaite, A.L., 2015. Seasonal variation in phosphorus concentration–
478 discharge hysteresis inferred from high-frequency in situ monitoring. *J. Hydrol.* 524,
479 333–347. <https://doi.org/10.1016/j.jhydrol.2015.02.036>
- 480 Bieroza, M.Z., Heathwaite, A.L., 2016. Unravelling organic matter and nutrient
481 biogeochemistry in groundwater-fed rivers under baseflow conditions: Uncertainty in in
482 situ high-frequency analysis. *Sci. Total Environ.* 572, 1520–1533.
483 <https://doi.org/10.1016/j.scitotenv.2016.02.046>
- 484 Bieroza, M.Z., Heathwaite, A.L., Bechmann, M., Kyllmar, K., Jordan, P., 2018. The
485 concentration-discharge slope as a tool for water quality management. *Sci. Total*
486 *Environ.* 630, 738–749. <https://doi.org/10.1016/j.scitotenv.2018.02.256>
- 487 Bol, R., Gruau, G., Mellander, P.-E., Dupas, R., Bechmann, M., Skarbøvik, E., Bieroza, M.,
488 Djodjic, F., Glendell, M., Jordan, P., Van der Grift, B., Rode, M., Smolders, E.,
489 Verbeeck, M., Gu, S., Klumpp, E., Pohle, I., Fresne, M., Gascuel-Oudou, C., 2018.
490 Challenges of Reducing Phosphorus Based Water Eutrophication in the Agricultural
491 Landscapes of Northwest Europe. *Front. Mar. Sci.* 5, 0–16.
492 <https://doi.org/10.3389/fmars.2018.00276>
- 493 Cassidy, R., Jordan, P., 2011. Limitations of instantaneous water quality sampling in surface-
494 water catchments: Comparison with near-continuous phosphorus time-series data. *J.*

495 Hydrol. 405, 182–193. <https://doi.org/10.1016/j.jhydrol.2011.05.020>

496 Cerdan, O., Govers, G., Le Bissonnais, Y., Van Oost, K., Poesen, J., Saby, N., Gobin, A.,
 497 Vacca, A., Quinton, J., Auerswald, K., Klik, A., Kwaad, F.J.P.M., Raclot, D., Ionita, I.,
 498 Rejman, J., Rousseva, S., Muxart, T., Roxo, M.J., Dostal, T., 2010. Rates and spatial
 499 variations of soil erosion in Europe: A study based on erosion plot data. *Geomorphology*
 500 122, 167–177. <https://doi.org/10.1016/j.geomorph.2010.06.011>

501 CLC2006, 2006. Corine Land Cover. [https://land.copernicus.eu/pan-european/corine-land-](https://land.copernicus.eu/pan-european/corine-land-cover)
 502 [cover.](https://land.copernicus.eu/pan-european/corine-land-cover)

503 Curie, F., Ducharne, A., Bendjoudi, H., Billen, G., 2011. Spatialization of denitrification by
 504 river corridors in regional-scale watersheds: Case study of the Seine river basin. *Phys.*
 505 *Chem. Earth* 36, 530–538. <https://doi.org/10.1016/j.pce.2009.02.004>

506 Delmas, M., Saby, N., Arrouays, D., Dupas, R., Lemercier, B., Pellerin, S., Gascuel-Oudou, C.,
 507 2015. Explaining and mapping total phosphorus content in French topsoils. *Soil Use*
 508 *Manag.* 31, 259–269. <https://doi.org/10.1111/sum.12192>

509 Diamond, J.S., Cohen, M.J., 2018. Complex patterns of catchment solute-discharge
 510 relationships for coastal plain rivers. *Hydrol. Process.* 32, 388–401.
 511 <https://doi.org/10.1002/hyp.11424>

512 Doublet, S., Le Gall, P., 2013. NOPOLU-Agri. Outil de spatialisation des pressions de
 513 l’agriculture. Méthodologie et résultats pour les surplus d’azote et les émissions des gaz
 514 à effet de serre. Campagne 2010-2011.

515 Duncan, J.M., Band, L.E., Groffman, P.M., 2017a. Variable nitrate concentration–discharge
 516 relationships in a forested watershed. *Hydrol. Process.* 31, 1817–1824.
 517 <https://doi.org/10.1002/hyp.11136>

518 Duncan, J.M., Band, L.E., Groffman, P.M., Bernhardt, E.S., 2015. Mechanisms driving the
 519 seasonality of catchment scale nitrate export: Evidence for riparian ecohydrologic
 520 controls. *Water Resour. Res.* 51, 3982–3997. <https://doi.org/10.1002/2015WR016937>

521 Duncan, J.M., Welty, C., Kemper, J.T., Groffman, P.M., Band, L.E., 2017b. Dynamics of
 522 nitrate concentration-discharge patterns in an urban watershed. *Water Resour. Res.* 53,
 523 7349–7365. <https://doi.org/10.1002/2017WR020500>

524 Dupas, R., Abbott, B.W., Minaudo, C., Fovet, O., 2019a. Distribution of landscape units
 525 within catchments influences nutrient export dynamics. *Front. Environ. Sci.* 7, 43.
 526 <https://doi.org/10.3389/FENV.S.2019.00043>

527 Dupas, R., Delmas, M., Dorioz, J., Garnier, J., 2015a. Assessing the impact of agricultural
 528 pressures on N and P loads and eutrophication risk. *Ecol. Indic.* 48, 396–407.
 529 <https://doi.org/10.1016/j.ecolind.2014.08.007>

530 Dupas, R., Gascuel-Oudou, C., Gilliet, N., Grimaldi, C., Gruau, G., 2015b. Distinct export
 531 dynamics for dissolved and particulate phosphorus reveal independent transport
 532 mechanisms in an arable headwater catchment. *Hydrol. Process.* 29, 3162–3178.
 533 <https://doi.org/10.1002/hyp.10432>

534 Dupas, R., Gruau, G., Gu, S., Humbert, G., Jaffrézic, A., Gascuel-Oudou, C., 2015c.
 535 Groundwater control of biogeochemical processes causing phosphorus release from
 536 riparian wetlands. *Water Res.* 84, 307–314. <https://doi.org/10.1016/j.watres.2015.07.048>

- 537 Dupas, R., Jomaa, S., Musolff, A., Borchardt, D., Rode, M., 2016. Disentangling the
538 influence of hydroclimatic patterns and agricultural management on river nitrate
539 dynamics from sub-hourly to decadal time scales. *Sci. Total Environ.* 571, 791–800.
540 <https://doi.org/10.1016/j.scitotenv.2016.07.053>
- 541 Dupas, R., Minaudo, C., Abbott, B.W., 2019b. Stability of spatial patterns in water chemistry
542 across temperate ecoregions. *Environ. Res. Lett.* [https://doi.org/10.1088/1748-](https://doi.org/10.1088/1748-9326/ab24f4)
543 [9326/ab24f4](https://doi.org/10.1088/1748-9326/ab24f4)
- 544 Dupas, R., Musolff, A., Jawitz, J.W., Rao, P.S.C., Jäger, C.G., Fleckenstein, J.H., Rode, M.,
545 Borchardt, D., 2017. Carbon and nutrient export regimes from headwater catchments to
546 downstream reaches. *Biogeosciences* 14, 4391–4407. [https://doi.org/10.5194/bg-14-](https://doi.org/10.5194/bg-14-4391-2017)
547 [4391-2017](https://doi.org/10.5194/bg-14-4391-2017)
- 548 Dupas, R., Tittel, J., Jordan, P., Musolff, A., Rode, M., 2018. Non-domestic phosphorus
549 release in rivers during low-flow: Mechanisms and implications for sources
550 identification. *J. Hydrol.* 560, 141–149. <https://doi.org/10.1016/j.jhydrol.2018.03.023>
- 551 Eckhardt, K., 2008. A comparison of baseflow indices, which were calculated with seven
552 different baseflow separation methods. *J. Hydrol.* 352, 168–173.
553 <https://doi.org/10.1016/j.jhydrol.2008.01.005>
- 554 Fovet, O., Humbert, G., Dupas, R., Gascuel-Oudou, C., Gruau, G., Jaffrezic, A., Thelusma,
555 G., Faucheux, M., Gilliet, N., Hamon, Y., Grimaldi, C., 2018. Seasonal variability of
556 stream water quality response to storm events captured using high-frequency and multi-
557 parameter data. *J. Hydrol.* 559, 282–293. <https://doi.org/10.1016/j.jhydrol.2018.02.040>
- 558 Fox, G.A., Purvis, R.A., Penn, C.J., 2016. Streambanks: A net source of sediment and
559 phosphorus to streams and rivers. *J. Environ. Manage.* 181, 602–614.
560 <https://doi.org/10.1016/j.jenvman.2016.06.071>
- 561 Godsey, S.E., Kirchner, J.W., Clow, D.W., 2009. Concentration–discharge relationships
562 reflect chemostatic characteristics of US catchments. *Hydrol. Process.* 23, 1844–1864.
563 <https://doi.org/10.1002/hyp.7315>
- 564 Gu, S., Gruau, G., Dupas, R., Rumpel, C., Crème, A., Fovet, O., Gascuel-Oudou, C.,
565 Jeanneau, L., Humbert, G., Petitjean, P., 2017. Release of dissolved phosphorus from
566 riparian wetlands: Evidence for complex interactions among hydroclimate variability,
567 topography and soil properties. *Sci. Total Environ.* 598, 421–431.
568 <https://doi.org/10.1016/j.scitotenv.2017.04.028>
- 569 Gu, S., Gruau, G., Malique, F., Dupas, R., Petitjean, P., Gascuel-Oudou, C., 2018.
570 Drying/rewetting cycles stimulate release of colloidal-bound phosphorus in riparian
571 soils. *Geoderma* 321, 32–41. <https://doi.org/10.1016/j.geoderma.2018.01.015>
- 572 Halliday, S.J., Skeffington, R. a., Wade, A.J., Bowes, M.J., Gozzard, E., Newman, J.R.,
573 Loewenthal, M., Palmer-Felgate, E.J., Jarvie, H.P., 2015. High-frequency water quality
574 monitoring in an urban catchment: hydrochemical dynamics, primary production and
575 implications for the Water Framework Directive. *Hydrol. Process.* 29, 3388–3407.
576 <https://doi.org/10.1002/hyp.10453>
- 577 Hipel, K.W., McLeod, A.I., 2005. *Time Series Modelling of Water Resources and*
578 *Environmental Systems.* [http://www.stats.uwo.ca/faculty/aim/1994Book/.](http://www.stats.uwo.ca/faculty/aim/1994Book/)
- 579 Hirsch, R.M., 2014. Large Biases in Regression-Based Constituent Flux Estimates: Causes

580 and Diagnostic Tools. *JAWRA J. Am. Water Resour. Assoc.* 50, 1401–1424.
581 <https://doi.org/10.1111/jawr.12195>

582 Hrachowitz, M., Benettin, P., Breukelen, B.M. Van, Fovet, O., Howden, N.J.K., Ruiz, L.,
583 Velde, Y. Van Der, Wade, A.J., 2016. Transit times - the link between hydrology and
584 water quality at the catchment scale. *WIREs Water* 3, 629–657.
585 <https://doi.org/10.1002/wat2.1155>

586 Jarvie, H.P., Sharpley, A.N., Scott, J.T., Haggard, B.E., Bowes, M.J., Massey, L.B., 2012.
587 Within-River Phosphorus Retention: Accounting for a Missing Piece in the Watershed
588 Phosphorus Puzzle. *Environ. Sci. Technol.* 46, 13284–13292.
589 <https://doi.org/10.1021/es303562y>

590 Jawitz, J.W., Mitchell, J., 2011. Temporal inequality in catchment discharge and solute
591 export. *Water Resour. Res.* 47, n/a-n/a. <https://doi.org/10.1029/2010WR010197>

592 Johnes, P.J., 2007. Uncertainties in annual riverine phosphorus load estimation: Impact of
593 load estimation methodology, sampling frequency, baseflow index and catchment
594 population density. *J. Hydrol.* 332, 241–258.
595 <https://doi.org/10.1016/j.jhydrol.2006.07.006>

596 Kim, H., Dietrich, W.E., Thurnhoffer, B.M., Bishop, J.K.B., Fung, I.Y., 2017. Controls on
597 solute concentration-discharge relationships revealed by simultaneous hydrochemistry
598 observations of hillslope runoff and stream flow: The importance of critical zone
599 structure. *Water Resour. Res.* 1–20. <https://doi.org/10.1002/2016WR019722>

600 Koenig, L.E., Shattuck, M.D., Snyder, L.E., Potter, J.D., McDowell, W.H., 2017.
601 Deconstructing the Effects of Flow on DOC, Nitrate, and Major Ion Interactions Using a
602 High-Frequency Aquatic Sensor Network. *Water Resour. Res.* 655–673.
603 <https://doi.org/10.1002/2017WR020739>

604 Li, W., Liu, H., Zhai, L., Yen, H., Hu, W., Lei, Q., Stewart, R.J., Guo, S., Ren, T., 2019.
605 Evaluation of concentration-discharge dynamics and nitrogen export on anthropogenic
606 inputs and stormflow across alternative time-scales. *Ecol. Indic.* 98, 879–887.
607 <https://doi.org/10.1016/j.ecolind.2018.11.057>

608 LITHO, 2008. dataset - <http://www.geocatalogue.fr/Detail.do?id=6388>.

609 Lyne, V.D., Hollick, M., 1979. Stochastic time-variable rainfall-runoff modelling. *Inst. Eng.*
610 *Aust. Natl. Conf.* 89–93.

611 McDonnell, J.J., Beven, K., 2014. Debates-The future of hydrological sciences: A (common)
612 path forward? A call to action aimed at understanding velocities, celerities and residence
613 time distributions of the headwater hydrograph. *Water Resour. Res.* 50, 5342–5350.
614 <https://doi.org/10.1002/2013WR015141>

615 Minaudo, C., Curie, F., Jullian, Y., Gassama, N., Moatar, F., 2018. QUAL-NET, a high
616 temporal-resolution eutrophication model for large hydrographic networks.
617 *Biogeosciences* 15, 2251–2269. <https://doi.org/10.5194/bg-15-2251-2018>

618 Minaudo, C., Dupas, R., Gascuel-Oudou, C., Fovet, O., Mellander, P.-E., Jordan, P., Shore,
619 M., Moatar, F., 2017. Nonlinear empirical modeling to estimate phosphorus exports
620 using continuous records of turbidity and discharge. *Water Resour. Res.* 53, 7590–7606.
621 <https://doi.org/10.1002/2017WR020590>

622 Minaudo, C., Meybeck, M., Moatar, F., Gassama, N., Curie, F., 2015. Eutrophication

623 mitigation in rivers: 30 years of trends in spatial and seasonal patterns of
624 biogeochemistry of the Loire River (1980–2012). *Biogeosciences* 12, 2549–2563.
625 <https://doi.org/10.5194/bg-12-2549-2015>

626 Moatar, F., Abbott, B.W., Minaudo, C., Curie, F., Pinay, G., 2017. Elemental properties,
627 hydrology, and biology interact to shape concentration-discharge curves for carbon,
628 nutrients, sediment, and major ions. *Water Resour. Res.* 53, 1–18.
629 <https://doi.org/10.1002/2016WR019635>

630 Moatar, F., Meybeck, M., 2005. Compared performances of different algorithms for
631 estimating annual nutrient loads discharged by the eutrophic River Loire. *Hydrol.*
632 *Process.* 19, 429–444. <https://doi.org/10.1002/hyp.5541>

633 Moatar, F., Meybeck, M., Raymond, S., Birgand, F., Curie, F., 2013. River flux uncertainties
634 predicted by hydrological variability and riverine material behaviour. *Hydrol. Process.*
635 27, 3535–3546. <https://doi.org/10.1002/hyp.9464>

636 Musolff, A., Fleckenstein, J.H., Rao, P.S.C., Jawitz, J.W., 2017. Emergent archetype patterns
637 of coupled hydrologic and biogeochemical responses in catchments. *Geophys. Res. Lett.*
638 44, 4143–4151. <https://doi.org/10.1002/2017GL072630>

639 Musolff, A., Schmidt, C., Rode, M., Lischeid, G., Weise, S.M., Fleckenstein, J.H., 2016.
640 Groundwater head controls nitrate export from an agricultural lowland catchment. *Adv.*
641 *Water Resour.* 96, 95–107. <https://doi.org/10.1016/j.advwatres.2016.07.003>

642 Musolff, A., Schmidt, C., Selle, B., Fleckenstein, J.H., 2015. Catchment controls on solute
643 export. *Adv. Water Resour.* 86, 133–146.
644 <https://doi.org/10.1016/j.advwatres.2015.09.026>

645 Nathan, R.J., McMahon, T.A., 1990. Evaluation of automated techniques for base flow and
646 recession analyses. *Water Resour. Res.* 26, 1465–1473.
647 <https://doi.org/10.1029/WR026i007p01465>

648 Pinay, G., Roques, L., Fabre, A., 1993. Spatial and temporal patterns of denitrification in a
649 riparian forest. *J. Appl. Ecol.* 30, 581–591. <https://doi.org/10.2307/2404238>

650 Powers, S.M., Bruulsema, T.W., Burt, T.P., Chan, N.I., Elser, J.J., Haygarth, P.M., Howden,
651 N.J.K., Jarvie, H.P., Lyu, Y., Peterson, H.M., Sharpley, A.N., Shen, J., Worrall, F.,
652 Zhang, F., 2016. Long-term accumulation and transport of anthropogenic phosphorus in
653 three river basins. *Nat. Geosci.* 9, 353–356. <https://doi.org/10.1038/ngeo2693>

654 Quintana-Segui, P., Le Moigne, P., Durand, Y., Martin, E., Habets, F., Baillon, M., Canellas,
655 C., Franchisteguy, L., Morel, S., 2008. Analysis of near-surface atmospheric variables:
656 Validation of the SAFRAN analysis over France. *J. Appl. Meteorol. Climatol.* 47, 92–
657 107. <https://doi.org/10.1175/2007JAMC1636.1>

658 R Core Team, 2016. R Core Team (2016). R: A language and environment for statistical
659 computing. R Foundation for Statistical Computing, Vienna, Austria.

660 Raymond, S., Moatar, F., Meybeck, M., Bustillo, V., 2013. Choosing methods for estimating
661 dissolved and particulate riverine fluxes from monthly sampling. *Hydrol. Sci. J.* 58,
662 1326–1339. <https://doi.org/10.1080/02626667.2013.814915>

663 Rode, M., Wade, A.J., Cohen, M.J., Hensley, R.T., Bowes, M.J., Kirchner, J.W., Arhonditsis,
664 G.B., Jordan, P., Kronvang, B., Halliday, S.J., Skeffington, R.A., Rozemeijer, J.C.,
665 Aubert, A.H., Rinke, K., Jomaa, S., 2016. Sensors in the Stream: The High-Frequency

- 666 Wave of the Present. *Environ. Sci. Technol.* 50, 10297–10307.
667 <https://doi.org/10.1021/acs.est.6b02155>
- 668 Rose, L.A., Karwan, D.L., Godsey, S.E., 2018. Concentration-discharge relationships
669 describe solute and sediment mobilization, reaction, and transport at event and longer
670 timescales. *Hydrol. Process.* 1–16. <https://doi.org/10.1002/hyp.13235>
- 671 Rozemeijer, J.C., Van Der Velde, Y., Van Geer, F.C., De Rooij, G.H., Torfs, P.J.J.F., Broers,
672 H.P., 2010. Improving load estimates for NO₃ and P in surface waters by characterizing
673 the concentration response to rainfall events. *Environ. Sci. Technol.* 44, 6305–6312.
674 <https://doi.org/10.1021/es101252e>
- 675 Smolders, E., Baetens, E., Verbeeck, M., Nawara, S., Diels, J., Verdrievael, M., Peeters, B., De
676 Cooman, W., Baken, S., 2017. Internal Loading and Redox Cycling of Sediment Iron
677 Explain Reactive Phosphorus Concentrations in Lowland Rivers. *Environ. Sci. Technol.*
678 51, 2584–2592. <https://doi.org/10.1021/acs.est.6b04337>
- 679 Snoubra, B., 2013. Les surplus d'azote et les gaz à effet de serre de l'activité agricole en
680 France métropolitaine en 2010. *Chiffres Stat. Serv. l'observation des Stat. Commis.*
681 *général au développement durable* 448.
- 682 Thompson, S.E., Basu, N.B., Lascrain, J., Aubeneau, A., Rao, P.S.C., 2011. Relative
683 dominance of hydrologic versus biogeochemical factors on solute export across impact
684 gradients. *Water Resour. Res.* 47, 1–20. <https://doi.org/10.1029/2010WR009605>
- 685 Tiwari, T., Lidman, F., Laudon, H., Lidberg, W., Ågren, A.M., 2017. GIS-based prediction of
686 stream chemistry using landscape composition, wet areas, and hydrological flow
687 pathways. *J. Geophys. Res. Biogeosciences* 122, 65–79.
688 <https://doi.org/10.1002/2016JG003399>
- 689 Underwood, K.L., Rizzo, D.M., Schroth, A.W., Dewoolkar, M.M., 2017. Evaluating Spatial
690 Variability in Sediment and Phosphorus Concentration-Discharge Relationships Using
691 Bayesian Inference and Self-Organizing Maps. *Water Resour. Res.* 53, 10293–10316.
692 <https://doi.org/10.1002/2017WR021353>
- 693 Van Meter, K.J., Basu, N.B., 2015. Catchment legacies and time lags: A parsimonious
694 watershed model to predict the effects of legacy storage on nitrogen export. *PLoS One*
695 10, 1–22. <https://doi.org/10.1371/journal.pone.0125971>
- 696 Williams, M.R., King, K.W., Baker, D.B., Johnson, L.T., Smith, D.R., Fausey, N.R., 2016.
697 Hydrologic and biogeochemical controls on phosphorus export from Western Lake Erie
698 tributaries. *J. Great Lakes Res.* 42, 1403–1411. <https://doi.org/10.1016/j.jglr.2016.09.009>
- 699 Zhang, Q., Ball, W.P., 2017. Improving riverine constituent concentration and flux estimation
700 by accounting for antecedent discharge conditions. *J. Hydrol.* 547, 387–402.
701 <https://doi.org/10.1016/j.jhydrol.2016.12.052>
- 702 Zhang, Q., Brady, D.C., Boynton, W.R., Ball, W.P., 2015. Long-term trends of nutrients and
703 sediment from the nontidal Chesapeake watershed. *J. Am. Water Resour. Assoc.* 1–22.
704 <https://doi.org/10.1111/1752-1688.12327>
- 705 Zhang, Q., Harman, C.J., Ball, W.P., 2016. An improved method for interpretation of riverine
706 concentration-discharge relationships indicates long-term shifts in reservoir sediment
707 trapping. *Geophys. Res. Lett.* 43, 10,215-10,224. <https://doi.org/10.1002/2016GL069945>
- 708